EUROFUSION WPMST1-CP(16) 15140

N Vianello et al.

On filamentary transport in the TCV tokamak: addressing the role of the parallel connection length

Preprint of Paper to be submitted for publication in
Proceedings of 26th IAEA Fusion Energy Conference

This work has been carried out within the framework of the EUROfusion Consortium and has received funding from the Euratom research and training programme 2014-2018 under grant agreement No 633053. The views and opinions expressed herein do not necessarily reflect those of the European Commission.

On Filamentary Transport in the TCV Tokamak: Addressing the Role of the Parallel Connection Length

N. Vianello[1], C. Tsui[3, 2], C. Theiler[2], S. Allan[4], J. Boedo[3], B. Labit[2], H. Reimerdes[2], K. Verhaegh[5], W. Vijvers[6], N. Walkden[4], S. Costea[7], J. Kovacic[8], C. Ionita[7], V. Naulin[9], A. H. Nielsen[9], J. J. Rasmussen[9], B. Schneider[7], R. Schrittwieser[7], M. Spolaore[1], D. Carralero[10], J. Madsen[9], F. Militello[4], B. Lipschultz[5], the TCV team[2] and and the EUROfusion MST1 Team[*1]

[1]*Consorzio RFX, Padova, Italy,* [2]*Swiss Plasma Center (SPC), EPFL Lausanne, Switzerland,* [3]*UCSD, La Jolla, USA,* [4]*CCFE, Culham UK,* [5]*York Plasma Institute, University of York, York, UK,* [6]*FOM Institute DIFFER, The Netherlands,* [7]*Institute for Ion Physics and Applied Physics, Innsbruck, Austria,* [8]*Jozef Stefan Institute, Ljubljana,* [9]*DTU, Lyngby, Denmark,* [10]*Max-Plank-Institut fur Plasmaphysik, Garching, Germany*

Corresponding Author: nicola.vianello@igi.cnr.it

Abstract:

A set of experiments to address the role of parallel connection length in modifying Scrape Off Layer (SOL) filamentary transport has been performed on the TCV tokamak. The effort has been motivated by the well establish observations, supported by a variety of devices, of SOL density profile broadening in high density regimes, which has been attributed to an enhancement of cross-field filamentary transport with respect to parallel losses. The TCV's flexibility has been used for a scan of parallel connection length obtained through a modification of poloidal flux expansion (f_x) at the target while keeping density and other macroscopic parameters identical during the scan, with the consequence of almost doubling $L_{\parallel}$ at the two extremes of the scan. SOL profile evolution with fueling has also been investigated at different current levels and different magnetic equilibria (Lower/Upper Single Null and Double Null). These observations have been compared with the corresponding differences in filaments dynamics.

Introduction

Plasma Wall Interaction (PWI) is a subject of intense study in the context of fusion energy research for the understanding of heat loading, sputtering levels, and the lifetime of the Plasma Facing Components. Transport in the Scrape Off Layer (SOL) region is the result of a competition between losses parallel and perpendicular to the magnetic field. In recent years a great effort has been devoted to the interpretation of SOL transport, with clear impact also on future machines design [1]. Indeed, ITER and DEMO are expected to operate at a high fraction of Greenwald density. In this condition, the L-Mode SOL exhibits a broadening of the density profile (also named *profile shoulder*) [2–5], and preliminary results confirmed this behavior also in H-Mode ITER relevant scenarios [6]. Since the beginning [2], SOL profile broadening has been attributed to an enhancement of advective transport. It has to be considered that SOL transport is dominated by the radial outward propagation of intermittent convective structures, named *filaments* or *blobs* [7], which convey particles and energy towards the first wall. Basic models for filaments [8] describe their emergence and propagation by a combination of plasma polarization, due to the ∇B drift, and parallel closure. Different closure schemes have been proposed: the filament can be in the *sheath connected regime* where parallel current is limited by the sheath resistivity, or in the *inertial regime*, i.e. disconnected from the divertor plates as a consequence of high SOL collisionality or large X-Point magnetic shear [3]. It has been

[*] See appendix of H. Meyer et.al. (OV/P-12) Proc. 26th IAEA Fusion Energy Conf. 2016, Kyoto, Japan

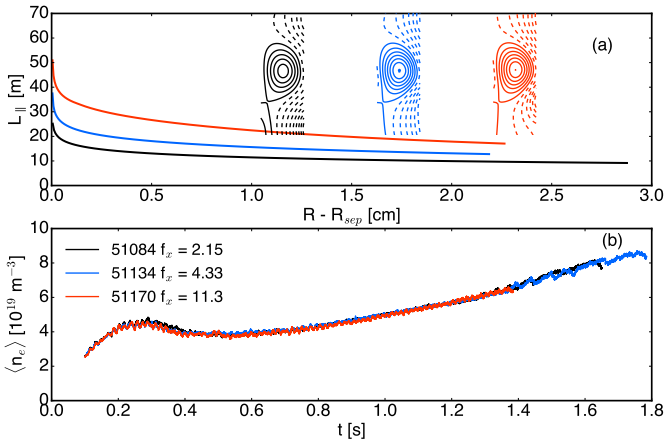

FIG. 1: Top: Parallel connection length from upstream to the outer target in three different discharges with different values of f_x. Bottom: Line average density $\langle n_e \rangle$ as a function of time

suggested that electrical connection could be also established through the plasma background [9]. Filaments in the two regimes exhibit different velocity scaling properties with respect to filament size [10]: the transition to the *inertial regime* can be accompanied by higher transport to the first wall at the midplane with potential issues for ITER. The effective collisionality parameter $\Lambda = \frac{L_\parallel}{c_s}\nu_{ei}\frac{\Omega_i}{\Omega_e}$, with $L_\parallel$ the parallel connection length, c_s the ion sound speed, ν_{ei} the electron-ion collision frequency and Ω_i, Ω_e the ion and electron gyrofrequency respectively, was introduced [10] to describe the transition between the two regimes at a fixed δ_b. Recent experimental observations from JET and AUG [11] suggested that in these two devices the SOL profile broadening is observed at the onset of the *intertial regime* occurring at $\Lambda = 1$, and that divertor conditions determine SOL shoulder formation [5]. Several experiments reported also that the density profiles are affected by plasma current (e.g. [12]) whereas the dependence on the divertor collisionality was less clear. These observations suggest a strong effect of the parallel connection length, with an easier broadening at longer connection length. So while it is clear that SOL profile and shoulder formation is a consequence of a change in the balance between cross-field and parallel transport, the real mechanism is still under investigation: this has motivated a detailed investigation on the TCV tokamak [13], where the high flexibility in plasma shaping has been used to address the effect of parallel connection length within this framework. Furthermore, considering the effect of magnetic topology on the SOL profiles observed on C-Mod [14], we have also performed investigations in Lower Single Null (LSN), Upper Single Nulle (USN) and Double Null (DN).

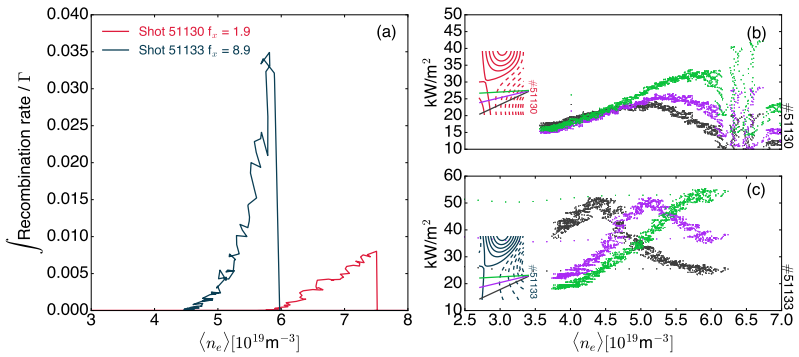

FIG. 2: (a) Integrated volumetric recombination rates as fraction of the ion flux to the target shown as function of line averaged density at two values of f_x. (b) Line integrated emissivity from bolometers at lower flux expansions as a function $\langle n_e \rangle$. (c) Same as panel (b) at higher value of f_x.

Flux expansion scan

Density ramp experiments were carried out in ohmically heated L-Mode plasma, where the flux expansion $f_x = (B_p/B_t)_{MP}/(B_p/B_t)_{SP}$, where B_p and B_t are respectively the poloidal and toroidal magnetic field computed at the Midplane (MP) or at the strike point (SP), has been varied in between shots from $f_x \approx 2$ to $f_x \approx 10$ by modification of the poloidal field at the target. A set of Lower Single Null (LSN) discharges was performed at different values of f_x with the same density ramp as shown in figure 1. The plasma current was 240 kA and the B_t was directed so that ion ∇B was pointing towards the X-point (*favorable* ∇B direction), which is a condition less favorable for detachment in TCV. From the geometrical point of view, the increase of the flux expansion causes an increase of the flux tube volume [15] as well as an increase of the parallel connection length between upstream and the target. The value of $L_{\parallel}$, computed from the midplane to the LFS target, is increased by up to 70% between the lower and the higher flux expansion cases as reported in Figure 1. In the early experiments [16] an enhanced degree of detachment was observed with increasing flux expansion and this was confirmed in recent experiments as well [17, 18], although it is worth mentioning that these observation was in *unfavorable* ∇B direction. From the experimental point of view, the volumetric integrated recombination rates have been determined for density ramp discharges from spectroscopic analysis of $n = 6, 7$ balmer line emission using the methodology described in [17]. The results, shown in figure 2 (a), indicate that the appearance of recombination occurs at lower core density for increased flux expansion cases. Additionally, for large flux expansion cases, higher recombination rates and higher divertor leg densities (as measured by Stark broadening) were achieved, despite the lower core density. This suggests that increased flux expansion can facilitate detachment. Confirmation can also be derived from bolometry, shown in panel (b) and (c) of the same Fig. 2, where we can observe that the emissivity front starts moving upwards towards the X-point earlier in density for the higher flux expansion case. Apart from the integral effect shown in Fig. 2, target profiles show clear differences in dependence on the Flux expansion. This is shown in the bottom panel of Fig. 3a where the target density profile is shown as a function of upstream-remapped distance from the separatrix for three discharges at the same average density but different flux expansion. The profile tends to broaden at the target in the higher f_x case as also shown in [18] although the core average density was approximately the same. In the top panel of the same figure the radial density profiles at the mid-plane, normalized to the density value at the separatrix, are shown. The profiles have been reconstructed using the

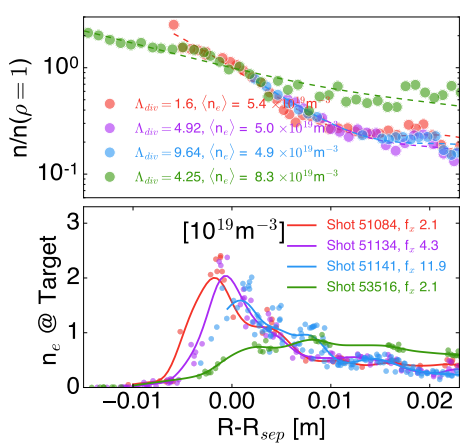

(a) Top: Normalized upstream density. Bottom: Target density as a distance from separatrix remapped at the midplane

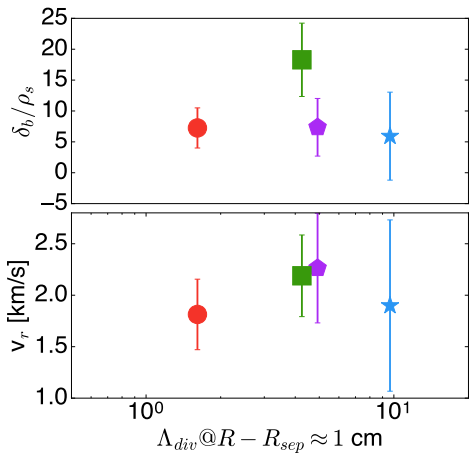

(b) Top: Normalized Blob dimension (top) and radial velocity (bottom) as a function of Λ_{div} computed at $R - R_{sep} \approx 1$cm.

FIG. 3: Analysis at different flux expansion

newly installed reciprocating probe on TCV, which has been previously exploited also on NSTX [19]. Temperature and density are derived using a double probe technique, whereas fluctuations are collected on ion saturation and floating potential pins, the latter arranged in order to provide poloidal and radial electric field from floating potential gradients. Considering the top panel of Figure 3 (a), no significant difference exists between the different flux expansion cases, despite the very large difference in the previously defined divertor normalized collisionality Λ_{div} (which is Λ computed with values of density and temperature at the target). This value is computed at $R - R_{sep} \approx 1$ cm, using as estimate for $L_{\parallel}$ the connection length from midplane to the target. This results represents an important difference with respect to the results reported in [11], where in a smaller range of Λ_{div} a huge variation of the profiles have been reported, and suggests that increasing the flux expansion does not provide any significant change in the upstream SOL in TCV despite the variation at the target. In order to obtain a clear broader profile the fueling must be increased even further as seen in the same Fig. 3a. It is worth noting that despite the close values in Λ_{div} between shots 51134 and 53516, the upstream and target profiles are very different suggesting that the total fueling rate is playing a major role in setting up the upstream profile.

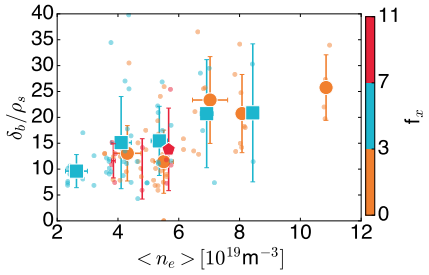

FIG. 4: Blob size normalized to local ion sound gyroradius computed at $R - R_{sep} \approx$ 1cm as a function of $\langle n_e \rangle$ with classes in f_x

In order to interpret upstream profile modification in the framework of filaments dynamics, blob size and velocity has been analyzed using the fast-reciprocating probe. The analysis has been performed using a standard conditional average technique as described for example in [7]: the blob size is computed from the FWHM size of the I_{sat} structure multiplied by the perpendicular velocity estimated as $v_{\perp} = \sqrt{v_r^2 + v_p^2}$, where the radial and poloidal component of the velocities are estimated from the fluctuations of poloidal and radial electric field gradient. The results of this analysis for the same three cases, shown as a function of Λ_{div} estimated approximately around 1cm from the separatrix, is shown in Figure 3b. The normalized collisionality varies by almost one order of magnitude, but despite this large variation the normalized blob size as well as the radial velocity are largely unaffected suggesting that the increase of parallel connection length by flux expansion is substantially inefficient in modifying filaments characteristics. On the other side filament is definitively larger in the case at higher fueling which exhibits a clear shoulder, confirming the relation between filaments size and profile flattening. This can also be confirmed on a statistical basis. For all the discharge in the database available we have computed the blob size normalized to the local ion sound gyroradius and we have studied the average density dependence distinguishing between classes in flux expansion. The blob size is found to increase with $\langle n_e \rangle$ with an almost linear trend and without any evidence of a threshold behavior. No difference can however be distinguished between the different f_x cases, supporting the previous statement.

Current scan

Motivated by the observations reported in MAST [12] and TCV [20], where, for a fixed density, profile broadening was clearer at lower plasma currents with respect to the higher ones, a set of discharges with similar density ramps were performed at different current levels still with the ion ∇B drift pointing towards the primary X-point. Figure 5a shows the upstream profile provided by the reciprocating probe as a function of distance from the separatrix at different densities and for different currents. As can be seen the slight density profile variation observed for $R - R_S \gtrsim 0.01$ at I_p = 160 kA can't be recognized at I_p = 240 kA, although similar levels of normalized Greenwald fraction are explored. In order to recover evidence of a SOL broadening

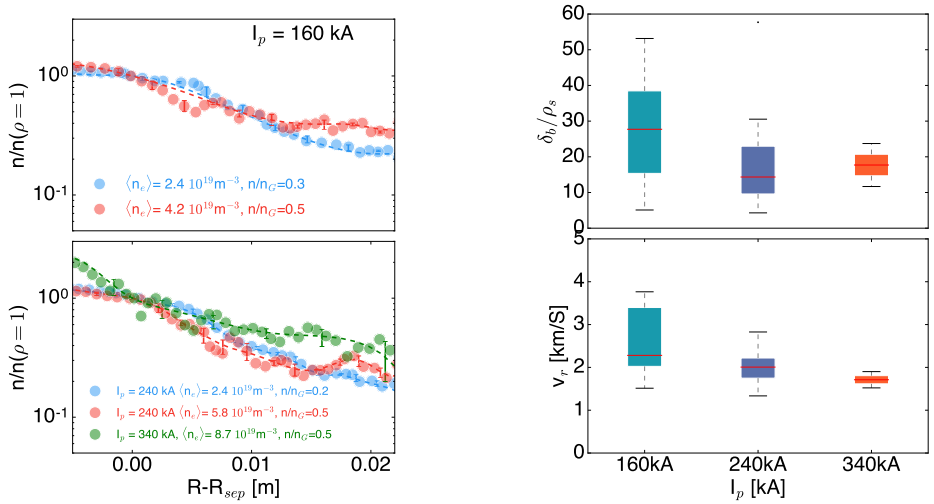

(a) *(b)*

FIG. 5: (a) Upstream density at different levels of density and current (b) Box and whiskers plot of normalized blob dimension (top) and filament radial velocity (bottom) at $R - R_{sep} \approx 1$ cm. The box represents the spread of the data between first and third quartiles, the horizontal bars are the median of the data, whereas the whiskers indicate the minimum and maximum.

at higher current we need to increase the density even further. By comparing the case at 240 kA and 340 kA we could infer that what is needed is the increase of fueling and corresponding average density as the 240 and 340 kA cases reach the same Greenwald fraction ($n_G[10^{20}\mathrm{m}^{-3}] = I_p[\mathrm{MA}]/(\pi a^2[\mathrm{m}^2])$) but with clear differences in the SOL profile. It is worth noting current increase causes a substantial reduction of $\mathrm{L}_{\parallel}$ in the SOL thus enhancing the emptying of the filaments through parallel advection. Correspondingly we need to increase the fueling level to obtain a similar upstream effect as observed also in [21]. This suggests in any case $\mathrm{L}_{\parallel}$ might play a role in the process of SOL profile broadening. A detailed filament characterization has been performed in a wider database of discharges distinguishing different levels of current but with similar shape and density between 0.3 and 0.5 n/n_G (thus neglecting the $n/n_G = 0.2$ case shown in Figure 5a). The statistical summary of these observations is shown in Figure 5b where blob size and radial velocity are shown and classified according to the current level. The blob size does not exhibit any clear trends whereas a small reduction of the radial velocity can be recognized at higher current. These results can be compared with [22] where both the radial size and velocity are found to decrease with increasing I_p.

Single and Double null

A dynamical investigation of the differences between single and double null divertor configuration has been also performed in within a single discharge. A set of discharges has been realized at I_p = 240kA and forward B_t direction, where starting from a LSN configuration, keeping both density and current constant throughout the discharge, a second X-point is brought into the vessel ending up in a connected Double Null (DN) configuration where the upper and lower single nulls lie on the same flux surface.

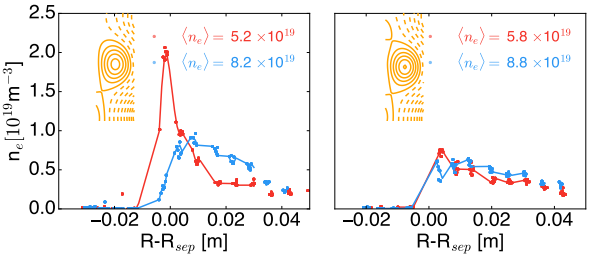

FIG. 6: Lower target density profiles in LSN (left) and DN (right) configuration at two levels of density

We investigated two levels of density, $\langle n_e \rangle \approx 5.2$ and 8.4 $\times 10^{19}\mathrm{m}^{-3}$ corresponding to 0.4 and 0.67 in Greenwald fraction, respectively. The introduction of the second X-point modifies

substantially the condition at the lower target, with a decrease of the density peak seen at $\langle n_e \rangle \approx 5.2 \times 10^{19}$ to values similar to the case at higher density. This can be shown by comparing the target density profiles in the four cases in Fig. 6. The same analysis cannot be performed for the Upper divertor, as TCV is not equipped with Langmuir probes on the ceiling and in the upper part of the central column. Bolometry can be used in any case to infer information on the radiation level in the upper and lower divertor.

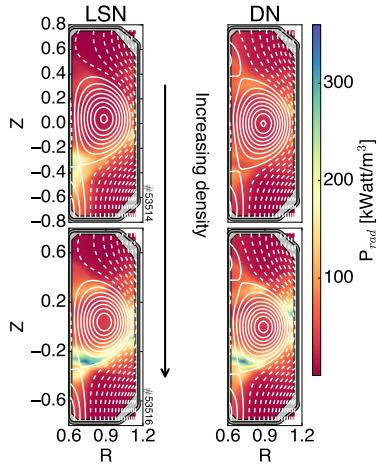

FIG. 7: Bolometric inversion in LSN and DN configuration at different densities

As it can be seen from Fig. 7 in the lower density and DN configuration case the radiation, is equally spread among the upper and lower X-Point whereas, if density is increased, higher radiation is always obtained in the lower divertor with a similar pattern in LSN and DN. This can probably be attributed to the fueling location which is always located on the floor in all the cases, or to drift effect that might determine which of the target detaches earlier. Upstream density profiles both in LSN and DN and at the two densities are compared in Figure 8 (a) normalized to the corresponding density at the separatrix. The comparison of the profiles in Fig. 8 (a) seems to indicate the tendency of the DN configuration to develop a slightly stronger shoulder in the region $0.5 \lesssim R - R_{sep} \lesssim 1.5$ cm, although we should note that we are also at a slightly higher density. In terms of filament dynamics, normalized blob size and radial velocities are shown in Figure 8b in both configurations. Within the error bar the radial velocity seems to be largely unaffected by the modification of equilibria and density, whereas a general increasing trend of blobs size with average density, already observed in Fig. 4, is observed, with the DN cases always slightly larger than the single null.

Upper/Lower/Double null

As a final step the same Ohmic density ramps at 240 kA have been repeated in Lower/Upper and Double null divertor configurations, where differing from the other cases the strike points have been kept at the inner wall for all the cases as can be seen in Fig. 9 (a). In this way we could estimate whether the fact that ∇B ion-drift points towards/away from the X-point, could have some influence on the SOL shoulder formation as can be partially inferred from C-Mod investigation [14]. Indeed in [14] it was observed that an Upper null configuration exhibits a

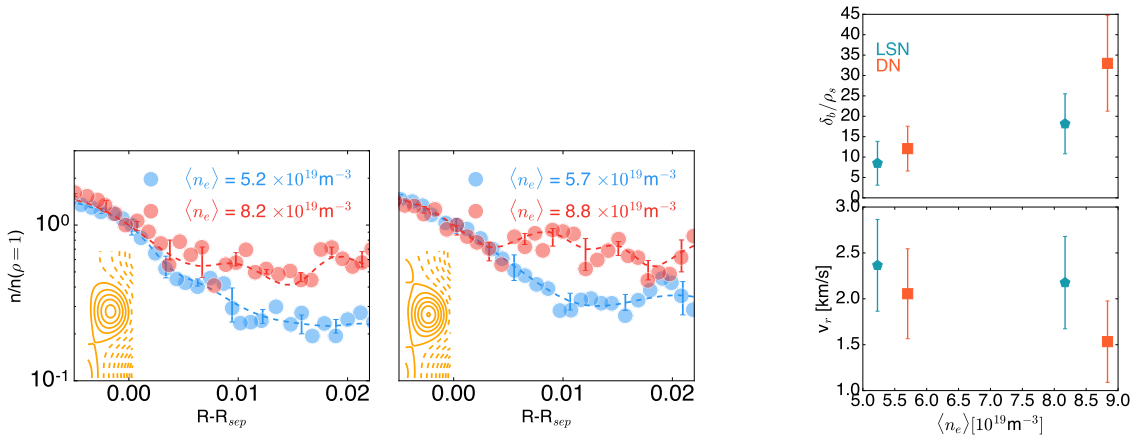

(a) *(b)*

FIG. 8: (a) Upstream density profile at different densities in the LSN (left) and (DN) configuration (b) Normalized blob size (top) and radial velocity of the filaments at $R - R_{sep} \approx 1$ cm in LSN and DN configuration.

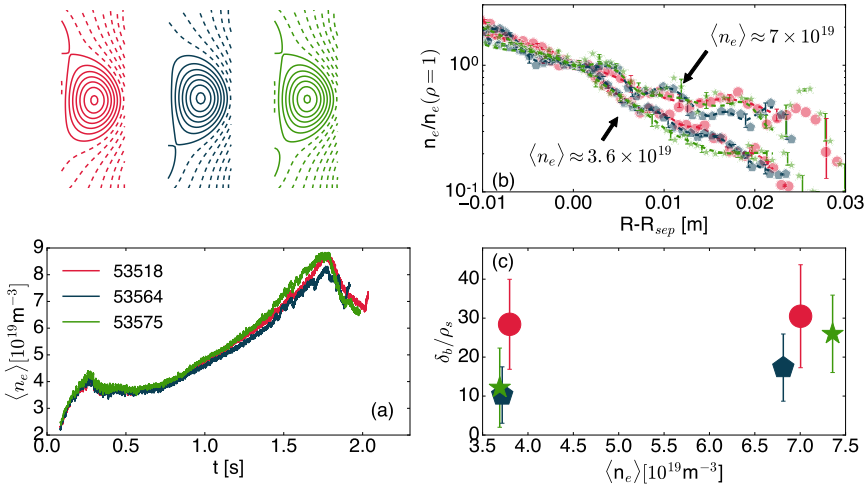

FIG. 9: (a) Line average density for Upper (red), lower (blue) and Double (green) null divertor configuration. The corresponding equilibria are shown in the upper panel (b) Upstream density profile normalized to $n_e(R_{sep})$ for the Upper (red), Lower (blue) and Double (green) null at two levels of density (c) Blob size normalized to local ρ_s estimated at $R - R_{sep} \approx 1$ cm in the three configuration as a function of average density

flatter profile at low and intermediate density, although the differences between configuration are weaker at higher density. The resulting profiles at the midplane are shown in figure 9 (b), all normalized to the corresponding values at the separatrix. In all three cases by increasing the density the midplane profile tends to broaden and no significant difference can be deduced among the three cases. In the bottom panel of the same figure 9 (c) the normalized blob sizes estimated at $R - R_{sep} \approx 1$ cm are shown for the three cases as a function of the line average density. Again, in LSN and DN configurations the filaments tend to increase their size as a function of density, as highlighted above. The Upper Single Null (USN) exhibits a larger size at low density without any clear modification when density is varied. But further investigations and more statistics are needed in order to gain confidence on this subject.

Summary and conclusion

In the attempt to summarize the results, the evolution of the density logarithmic scale $\lambda_n = |n_e/\nabla n_e|$ has been analyzed as a function of different parameters. The scale length has been determine starting from the profile and computing a weighted spline interpolation of the profile to get rid of the possible noise of the profile gradient. Examples of this type of spline are available throughout the paper (the dashed lines in the profile plots). This allows a better estimate of the gradients of the profile. In particular, to interpret the profile evolution in the framework of filaments dynamics, besides the aforementioned divertor collisionality, we have computed also

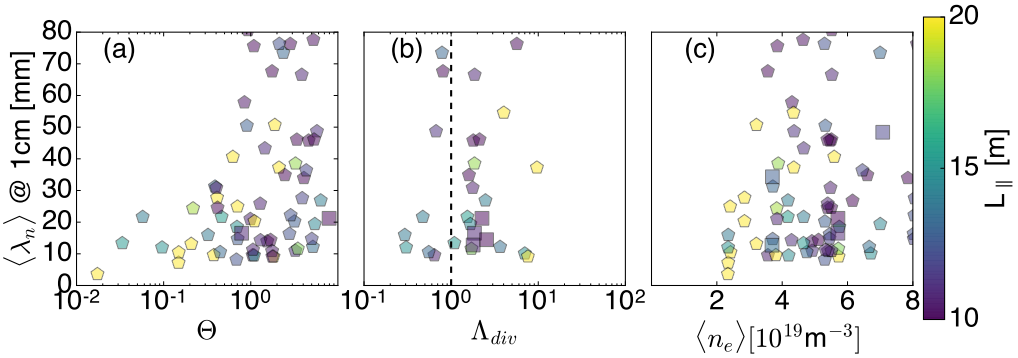

FIG. 10: (a) $\langle \lambda_n \rangle$ Evaluated evaluated between 0.8 and 1.5 cm from the separatrix as a function of (a) Θ, (b) Λ_{div}, (c) $\langle n_e \rangle$. The color code is proportional to the $L_{||}$ at the same radial location whereas pentagons indicate LSN equilibria and square the DN equilibria

the parameter Θ, defined in [10] as $\Theta = \hat{a}^{5/2} = \left(\frac{\delta_b R^{1/5}}{L_\parallel^{2/5}\rho_s^{4/5}}\right)^{5/2}$ which is a form of normalized blob size generally used in describing the parameter space in filament dynamics [10, 23]. The average value of λ_n as estimated between 0.8 and 1.5 cm from the separatrix, is shown as a function of Θ, Λ_{div} and $\langle n_e \rangle$ in figure 10 panel (a), (b) and (c) respectively. The spatial regions where the density scale length has been evaluated is where the density profile tends to exhibit a more pronounced shoulder in the various cases. Colors of the plotted symbols are proportional to the local estimate of the parallel connection length from the midplane to the floor, whereas the different symbols refer to different equilibria (pentagons are standard LSN with strike point on the floor whereas squares are DN). We clearly notice that the dependence of λ_n on the value of $L_\parallel$ is rather weak whereas it is clearer that flatter profiles are obtained for larger blobs, thus confirming the role of turbulence in establishing the upstream profile. It is also worth remembering that we have identified a clear dependence of the blob size on the line average density, whereas scanning the other paramenters like f_x did not provide a clear difference. The dependence on Λ_{div} is actually weaker than the one reported in [11] in particular for the points at very large Λ_{div} which can exhibit values of λ_n close to the ones at the extreme lower values. It is worth noting that differently from AUG and JET, where the data in [11] has been collected, the TCV wall is entirely covered with graphite tiles which exhibit a different recycling coefficient as compared with tungsten walls and divertors. Furthermore, TCV has a completely open divertor without baffles and all these characteristics implies a rather different neutral profile and neutral compression as compared with JET and AUG. So while the role of fluctuations in establishing SOL upstream profile are clearly confirmed by the present data, further investigation is needed to establish the exact mechanism including the role of neutrals in this complex phenomena.

Acknowledgment

This work has been carried out within the framework of the EUROfusion Consortium and has received funding from the Euratom research and training programme 2014-2018 under grant agreement No 633053. The views and opinions expressed herein do not necessarily reflect those of the European Commission.

References

[1] M. Kočan et al., Nucl. Fus. **55**, 033019 (2015).
[2] B. LaBombard et al., Phys. Plasmas **8**, 2107 (2001).
[3] D. L. Rudakov et al., Nucl. Fus. **45**, 1589 (2005).
[4] O. E. Garcia et al., Nucl. Fus. **47**, 667 (2007).
[5] D. Carralero et al., Nucl. Fusion **54**, 123005 (2014).
[6] H. W. Müller et al., Journ.Nucl.Mat. **463**, 739–743 (2015).
[7] J. A. Boedo et al., Phys. Plasmas **8**, 4826–4833 (2001).
[8] S. I. Krasheninnikov, Phys. Lett. A **283**, 368 (2001).
[9] L. Easy et al., Physics of Plasmas **21**, 122515 (2014).
[10] J. R. Myra et al., Physics of Plasmas **13**, 112502 (2006).
[11] D. Carralero et al., Phys. Rev. Let. **115**, 215002 (2015).
[12] F. Militello et al., Nuclear Fusion **56**, 016006 (2016).
[13] S. Coda et al., Nucl. Fus. **53**, 104011 (2013).
[14] B. LaBombard et al., Nuclear Fusion **44**, 1047–1066 (2004).
[15] V. A. Soukhanovskii et al., Journal of Nuclear Materials **438**, S96–S101 (2013).
[16] R. A. Pitts et al., Journ.Nucl.Mat. **290-293**, 940 (2001).
[17] K. Verhaegh et al., submitted to Nucl. Mat. Energy (2016).
[18] C. Theiler et al., submitted to Nucl. Fusion (2016).
[19] J. A. Boedo et al., Review of Scientific Instruments **80**, 123506 (2009).
[20] O. E. Garcia et al., Plasma Phys. Contr. Fus. **49**, B47 (2007).
[21] D. Carralero et al., Submitted to Nucl. Mat. Energy (2016).
[22] A. Kirk et al., Plasma Physics and Controlled Fusion **58**, 085008 (2016).
[23] D. A. Russell et al., Physics of Plasmas **14**, 102307 (2007).